

FFIBM/766/130

Kjeller 9 November 2000



Bjarne Haugstad
Director of Research

**BOUNDARY EFFECTS IN PENETRATION INTO
CONCRETE**

TELAND Jan Arild, SJØL Henrik

FFI/RAPPORT-2000/05414


FORSVARETS FORSKNINGSINSTITUTT
Norwegian Defence Research Establishment
Postboks 25, 2027 Kjeller, Norge

FORSVARETS FORSKNING SINSTITUTT (FFI)
Norwegian Defence Research Establishment
 P O BOX 25
 NO-2027 KJELLER, NORWAY

UNCLASSIFIED

SECURITY CLASSIFICATION OF THIS PAGE
 (when data entered)

REPORT DOCUMENTATION PAGE

1) PUBL/REPORT NUMBER FFI/RAPPORT-2000/05414 1a) PROJECT REFERENCE FFIBM/766/130	2) SECURITY CLASSIFICATION UNCLASSIFIED 2a) DECLASSIFICATION/DOWNGRADING SCHEDULE	3) NUMBER OF PAGES 34		
4) TITLE BOUNDARY EFFECTS IN PENETRATION INTO CONCRETE (RANDEFFEKTER VED PENETRASJON I BETONG)				
5) NAMES OF AUTHOR(S) IN FULL (surname first) TELAND Jan Arild, SJØL Henrik				
6) DISTRIBUTION STATEMENT Approved for public release. Distribution unlimited (Offentlig tilgjengelig)				
7) INDEXING TERMS IN ENGLISH: <table style="width: 100%; border: none;"> <tr> <td style="width: 50%; vertical-align: top;"> a) Penetration _____ b) Concrete _____ c) Boundary effects _____ d) Simulation _____ e) _____ </td> <td style="width: 50%; vertical-align: top;"> IN NORWEGIAN: a) Penetrasjon _____ b) Betong _____ c) Randeffekter _____ d) Simulering _____ e) _____ </td> </tr> </table>			a) Penetration _____ b) Concrete _____ c) Boundary effects _____ d) Simulation _____ e) _____	IN NORWEGIAN: a) Penetrasjon _____ b) Betong _____ c) Randeffekter _____ d) Simulering _____ e) _____
a) Penetration _____ b) Concrete _____ c) Boundary effects _____ d) Simulation _____ e) _____	IN NORWEGIAN: a) Penetrasjon _____ b) Betong _____ c) Randeffekter _____ d) Simulering _____ e) _____			
THESAURUS REFERENCE:				
8) ABSTRACT <p>Within the HPC project, several penetration experiments have been performed. In this report it is investigated whether boundary effects might have been present in some of these experiments. This is done by using a combination of analytical theory and numerical simulations. We also examine the phenomenon of boundary effects during penetration into concrete in general, and identify various effects that contribute in different ways. From simulations, boundary effects are seen to first appear when reflected waves from the boundary returns to the projectile. It is also shown that modelling the tensile failure correctly is important when boundary effects are present.</p>				
9) DATE 9 November 2000	AUTHORIZED BY This page only  Bjarne Haugstad	POSITION Director of Research		

CONTENTS

	Page
1	INTRODUCTION 4
2	PENETRATION EXPERIMENTS WITHIN THE HPC-PROJECT 4
3	PHYSICAL MECHANISMS 6
4	ANALYTICAL APPROACHES 7
4.1	Naive approach (extreme safety) 7
4.2	Modification of Forrestal's formula 8
4.3	Target resistance 8
4.4	Drawbacks of the analytical approach 11
5	AUTODYN SIMULATIONS 12
5.1	75 mm projectile against Densit 13
5.2	75 mm projectile against C150 14
5.3	75 mm projectile against standard concrete 16
5.4	152 mm projectile against Densit 16
5.5	152 mm projectile against C150 18
5.5.1	Results for a different C150 material model 20
5.6	152 mm projectile against standard concrete 21
5.7	Comparison of numerical and experimental results 23
6	FURTHER NUMERICAL ANALYSIS OF BOUNDARY EFFECTS 23
6.1	75 mm projectile against Densit 23
6.2	75 mm projectile against C30 25
7	RESULTS, RECOMMENDATIONS AND FURTHER WORK 26
	References 28
 APPENDIX	
A	CONCRETE DATA 29
A.1	C30 model 29
A.2	C150 model 29
A.3	Densit model 31
B	EXPERIMENTAL PENETRATION DATA 32
	Distribution list 33

BOUNDARY EFFECTS IN PENETRATION INTO CONCRETE

1 INTRODUCTION

In the HPC–project, which is a cooperation between various Norwegian and Swedish organizations, the properties of HPC (High Performance Concrete) are studied. An important part of the project has been penetration experiments where different projectiles have been fired against various concrete targets.

Penetration into concrete is an extremely complicated process, as there are many different variables/parameters contributing in some way to the final result. Such variables include material data for both projectile and target, shape of the projectile and impact velocity.

Another variable that could be important is the size of the target. Consider a situation where two identical projectiles are fired at the same impact velocity at targets of identical concrete quality, but different diameter. The penetration depth will then not necessarily be the same for both projectiles.

In fact, the projectile will penetrate further into the smallest target (provided that it is sufficiently small) than into the large target. Ideally, one would like to eliminate target size as a variable by performing the experiments against semi–infinite targets, but for practical reasons this is, of course, not possible. Large targets cost more money to manufacture, so instead one tries to design targets that are as small as possible, but still *sufficiently large* to avoid boundary effects.

But, how large is “sufficiently large”? This is a very difficult question to answer. In this document, an attempt is made at examining the phenomenon of boundary effects in general. However, we will restrict our attention to the penetration of rigid projectiles. Our obtained knowledge will be used to establish some guidelines for determining a sufficiently large target size and then check whether boundary effects were present in the HPC experiments.

2 PENETRATION EXPERIMENTS WITHIN THE HPC–PROJECT

Several large scale penetration experiments have over the years been performed within the framework of the HPC–project. These experiments have been performed with two different types of projectiles, namely of 75 mm and 152 mm diameter, both of which are shown in Figure 2.1. The projectiles always remained undeformed during the penetration process. Experimental data are given in Appendix B.

The 75 mm projectile had a mass of 6.28 kg, and a nose curvature radius of 140 mm. This corresponds to $\psi = r/d = 1.87$. The 152 mm projectile was an old anti–ship missile with a total mass of 44.76 kg and a truncated conical nose having a Forrestal nose factor $N=0.4$.

The projectiles were fired against a wide variety of concrete targets. Geometrically this included cylindrical, rectangular and layered targets of different diameters. The concrete used included various combinations at different compressive strengths, some containing fiber or steel reinforcement. Unfortunately, the large variety of targets made it somewhat difficult to compare the various experiments.



Figure 2.1: The 152 mm and 75 mm projectiles used in the HPC-experiments.

The experiments that will be particularly examined in this report were performed against cylindrical concrete targets of compressive strengths at 30, 150 and 200 MPa without reinforcement or fiber. Unfortunately, exact material data were not available for the C30 and C150 concrete, but a GREAC cell test of the C200 (Densit) concrete was performed at Imperial College (1), yielding static triaxial data. To model the C30 and C150 concrete, we have used triaxial material data for similar concretes with roughly the same compressive strength.

Most of the C30 and Densit concrete targets had diameters of around 160 cm. As a consequence, very little experimental data is available to confirm whether boundary effects were present in these experiments. Our analysis will therefore mostly be based on numerical analysis and analytical theory in these cases. For the C150 concrete, a more systematic experimental approach to investigate boundary effects was applied, which means that comparable experimental data is available for this concrete.

Already at an early stage, we can find some indications of boundary effects being present. It is convenient to define non-dimensional variables X and V , as this enables us to plot different experimental results in the same diagram.

$$X = x/d \quad , \quad V = \sqrt{\frac{m}{d^3 \sigma_c S}} v \quad , \quad S = 82.6 \left(\frac{\sigma_c}{10^6} \right)^{-0.544} \quad (2.1)$$

where the concrete compressive strength σ_c is measured in Pascal. Here m is the projectile mass, d the projectile diameter and x the final penetration depth.

In Figure 2.2 we have plotted all comparable data from the HPC experiments 1996–1999 for cylindrical targets of diameter 160 cm. Data for layered targets, targets with reinforcement and rectangular targets have therefore not been included.

Further, in Figure 2.2 we have also compared the results with predictions of Forrestal's penetration formula (2)–(3). However, it is important to be aware that these analytical penetration curves depend slightly on the concrete density. To avoid cluttering the figure with one graph for each concrete, we have only plotted the curves for C30. The density dependence is negligible for $V < 2.5$, which is where all the Densit data lie anyway.

It is seen from Figure 2.2 that the experimental data points lie above the analytical prediction for high impact velocities, while for low impact velocities the average agreement seems to be pretty good. Further, we notice that the Densit data (which all correspond to low values of V) seem to agree well with theory in all cases.

This might be an indication that boundary effects are present at high impact velocities for the weak C30 concrete, as Forrestal's formula has earlier been shown to give good agreement with various experiments (4) in this parameter range.

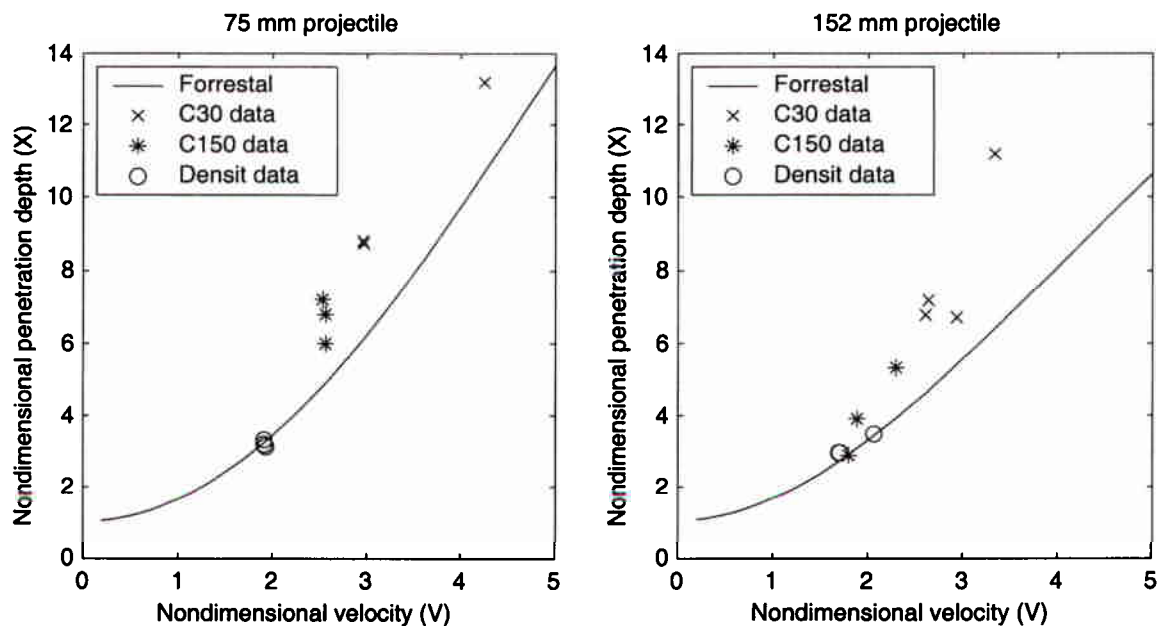


Figure 2.2: Comparison between Forrestal's penetration formula and experimental data from the HPC-project for 75 mm and 152 mm projectiles against various concrete targets.

3 PHYSICAL MECHANISMS

It is clear that, in some way, the small target offers less penetration resistance than the large target, even though the projectile trajectory is not near the target boundary. We are interested in discovering the physical mechanisms responsible for this effect.

Since the projectile itself is not near the boundary, the effect must be due to the generated stress field which propagates outwards from the projectile and eventually reaches the edge of the target.

There are several ways this could possibly influence the penetration process:

- When the compressive stress waves are reflected, they become tensile waves. Concrete is a material which can not withstand very much tension, so this reflection may lead to the concrete breaking up. If the concrete target contains micro or macro cracks, penetration might be easier due to modified material properties.
- Further, when the waves reach the boundary and are reflected as tensile waves, they eventually return to the (zone near the) projectile. This decreases the pressure (stress) near the projectile, and therefore also the force decelerating the projectile.
- Another possibility has to do with the “brittle plastic” zone that is created around the projectile. If the pressure is high enough, this plastic zone might reach the target boundary, in which case the target becomes completely unstable as there is no confinement (no elastic zone) to prevent it from “flowing” outwards. This should also increase penetration.

The physical mechanisms mentioned above should be the most important ones. The main problem is to figure out a criterion for dimensions of the target as a function of impact velocity, projectile and target properties.

4 ANALYTICAL APPROACHES

There exist some analytical approaches for determining the boundary effects. We begin our investigation by taking a look at these theories:

4.1 Naive approach (extreme safety)

One naive criterion for avoiding edge effects is that the target must be so large that the reflected stress waves don't have time to return. If the boundaries are very far from the penetration tunnel, the waves will take so long time to complete the round trip that penetration will have finished (the projectile will have come to rest) before they can interact in any way with the projectile. This should give an upper limit on the dimensions of the target, so that increasing the target size above this limit has no effect on the penetration depth.

However, assuming a sound velocity of 2500 m/s, which is quite typical for concrete, the waves will travel 2.5 meter for each millisecond. If the penetration process lasts, say 3 milliseconds, which is quite typical for experiments with the 152 mm projectile, a target with a diameter of around 7.5 meters is required to be absolutely sure there are no boundary effects.

Using this criterion we would hardly be able to get rid of the edge effects in any penetration experiment, which is pretty bad news since it would make the interpretation much

more difficult. However, even though the waves have returned, it is not certain that they will interact with the projectile to make penetration easier. We shall soon see that the naive condition might be unnecessary strict and that we probably can get away with having smaller targets.

4.2 Modification of Forrestal's formula

Forrestal's formula for penetration into semi-infinite concrete targets is seen to give good agreement with many different experiments, and is generally regarded as the best semi-analytical formula. Being based on cavity expansion, it assumes the following form for the force F_0 on the projectile during the tunneling phase of penetration:

$$F_0 = S\sigma_c + N\rho v^2 \quad (4.1)$$

where ρ is the concrete density. On non-dimensional form, this gives the following final penetration:

$$X_0 = \frac{2}{\pi} \left(\frac{M}{N} \right) \ln \left(\frac{M/N + V^2}{\pi/2 + M/N} \right) + 2, \quad M = \frac{m}{d^3\rho}, \quad N = N(r/d) \quad (4.2)$$

The question is now whether this formula can be modified to apply to penetration of a finite target with diameter d_t . The force F in this situation can generally be written as:

$$F = \alpha(v, x, d_t, \dots) F_0, \quad 0 < \alpha < 1 \quad (4.3)$$

where, as indicated, the relative penetration resistance α is not necessarily a constant, but may depend on the projectile velocity and penetration depth as well as other parameters describing the problem.

However, let us assume as a first approximation that α can be considered as independent of the velocity and penetration depth, and only as a function of the other parameters (target diameter, material model) which remain constant throughout the penetration process. Then the non-dimensional penetration depth X_t for a finite target is easily found to be given by:

$$X_t = \frac{2}{\alpha\pi} \frac{M}{N} \ln \left(\frac{M/N + V^2}{\alpha\frac{\pi}{2} + M/N} \right) + 2 \quad (4.4)$$

The question is now whether the assumptions made about α are reasonable, and whether it is possible to derive an explicit expression for α . A possible way of achieving this is described in the next section.

4.3 Target resistance

A quite interesting analytical work on boundary effects has been performed by Littlefield et.al. (5). Their idea was to incorporate boundary effects by modifying the theory of cavity expansion.

The purpose of cavity expansion theory is to derive an expression for the stresses induced in a material where a cavity is forced to expand. For a review of cavity expansion theory, see Teland (6). Usually only an infinite material is considered, but Littlefield examined a finite material to see how this changed the calculated stress distribution.

The calculated radial stress at the cavity boundary p_r was then used by Littlefield as an estimate for the empirical constant R_t in hydrodynamic long-rod penetration. Instead of looking at the high velocity case like Littlefield, we will below outline a first analytical approximation to model boundary effects for penetration of rigid projectiles.

In the regular penetration theory for rigid projectiles based on cavity expansion theory, the derived radial stress p_r is, through an integration process, used to calculate the total force on the projectile. The projectile acceleration, velocity and position is then found from Newton's 2nd law.

In principle the cavity can be assumed to have any possible shape, but in practice only cylindrical and spherical shape is considered.

As mentioned, when a finite boundary is considered, the expression for p_r becomes more complicated. Instead of the resistance only depending on the material parameters (and the geometry of the assumed cavity), there is now also a dependency on the target diameter d_t , the cavity diameter d and the diameter of the elastic-plastic zone d_{ep} . For quasistatic expansion and a Mises material model, we can calculate the expression explicitly.

In cylindrical cavity expansion theory, the result becomes (5):

$$p_r = \frac{Y}{\sqrt{3}} \left[1 - \left(\frac{d_{ep}}{d_t} \right)^2 + \ln \left(\frac{d_{ep}}{d} \right)^2 \right] \quad (4.5)$$

$$\left(\frac{d_{ep}}{d_t} \right)^2 = \frac{1}{2(1-2\nu)} \left[\sqrt{1 + \frac{4\sqrt{3}G}{Y}(1-2\nu) \left(\frac{d}{d_t} \right)^2} - 1 \right] \quad (4.6)$$

We see that as d_t grows large, the second term in the parenthesis approaches zero, and the penetration resistance p_r approaches the familiar expression from infinite cavity expansion theory:

$$\lim_{d_t/d \rightarrow \infty} p_r = p_r^0 = \frac{Y}{\sqrt{3}} \left[1 + \ln \left(\frac{\sqrt{3}G}{Y} \right) \right] \quad (4.7)$$

The corresponding results from spherical cavity expansion are:

$$p_r = \frac{2Y}{3} \left[1 - \left(\frac{d_{ep}}{d_t} \right)^3 + \ln \left(\frac{d_{ep}}{d} \right)^3 \right] \quad (4.8)$$

$$\left(\frac{d_{ep}}{d_t} \right)^3 = \frac{1}{4} \left(\frac{1+\nu}{1-\nu} \right) \left[\sqrt{1 + \frac{16G}{Y} \left(\frac{1-\nu}{1+\nu} \right) \left(\frac{d}{d_t} \right)^3} - 1 \right] \quad (4.9)$$

$$\lim_{d_t/d \rightarrow \infty} p_r = p_r^0 = \frac{2Y}{3} \left(1 + \ln \left(\frac{2G}{Y} \right) \right) \quad (4.10)$$

Our idea is now to approximate the relative penetration resistance α in the following way:

$$\alpha = \frac{p_r}{p_r^0} = \alpha \left(\frac{d_t}{d}, \nu, \frac{Y}{G} \right) \quad (4.11)$$

The relative penetration resistance α is seen to only depend on the three non-dimensional parameters: the ratio between target and projectile diameter d_t/d , the Poisson ratio ν and Y/G .

For most materials of interest, the Poisson ratio is in the range 0.2–0.3 and therefore does not vary that much. Likewise, for a material with a high yield limit, there usually is a correspondingly high shear modulus, so the ratio Y/G does not vary too much, either. This means that d_t/d is by far the most important parameter in determining the relative penetration resistance.

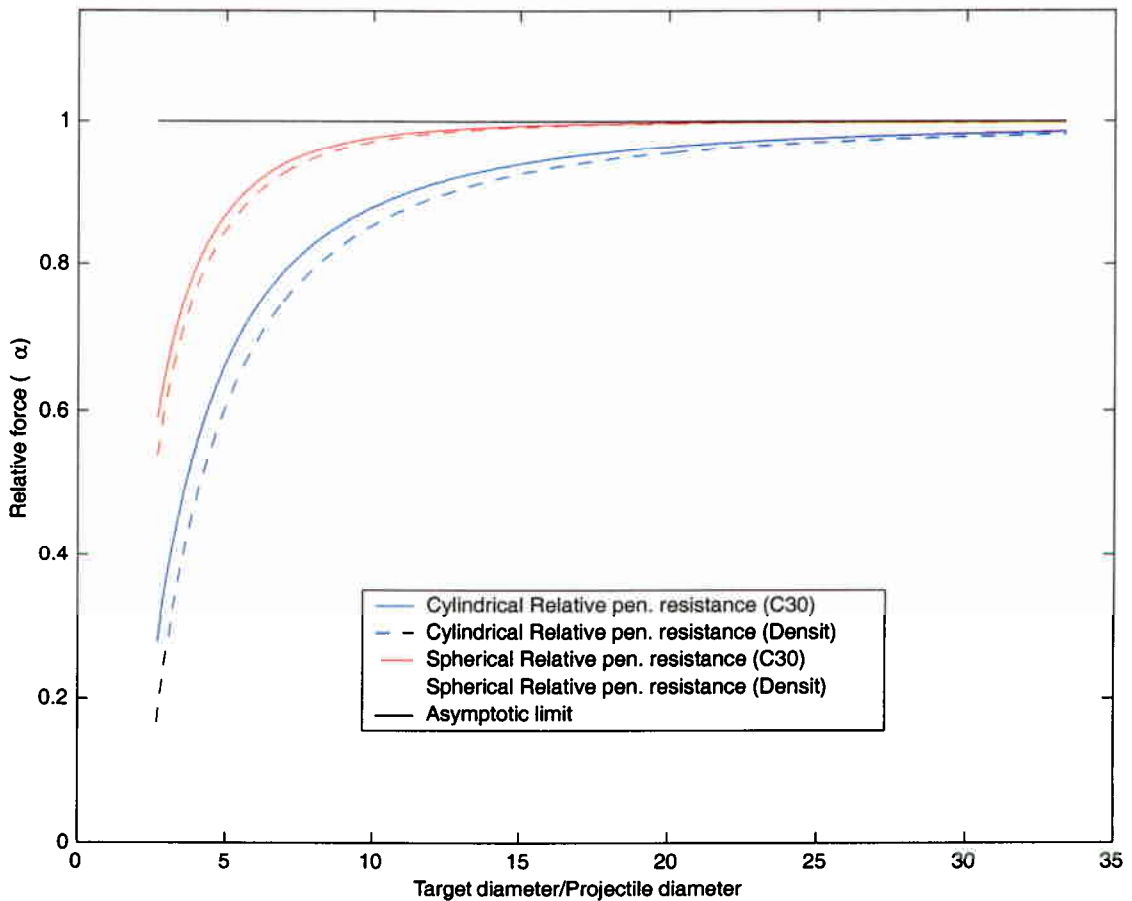


Figure 4.1: Penetration resistance as a function of ratio between target and projectile diameter.

To investigate further the dependence of α on the target diameter, we have plotted α as a function of d_t/d in Figure 4.1, both for spherical and cylindrical cavity expansion theory.

For the material parameters Y and G , we have used the values of $Y/G = 400 \text{ MPa}/15000 \text{ MPa} = 0.0266$ and $Y/G = 150 \text{ MPa}/4000 \text{ MPa} = 0.0375$, corresponding to Densit and C30 concrete under relatively high pressure.

We notice that there is a quite substantial difference between cylindrical and spherical theory. In cylindrical theory the dependence on target diameter is much stronger, thus giving larger boundary effects. We also note that there is not much difference in the relative penetration resistance for the two material models, as was mentioned earlier.

However, particularly in the cylindrical case, we see that for small target diameters the force is reduced quite significantly. The expressions approach the unmodified Forrestal formula asymptotically, and for d_t/d around 15, the difference is only around 10% for cylindrical and almost negligible for spherical theory.

In the following we will work with cylindrical theory as this seems more natural in this case.

4.4 Drawbacks of the analytical approach

The advantage of the analytical approach is that it provides a very simple analytical estimate of the increased penetration depth as a result of boundary effects.

There are some problems with this approach, though. Firstly, the expressions (4.5)–(4.6) and (4.8)–(4.9) have been derived for a very simple Mises material model. This means that it does not take reflection of waves and the effect of concrete's low tensile failure limit into account. Secondly, they are in principle only valid quasistatically, so a dynamic term should in general be included.

Further, concrete is best described by a pressure dependent yield curve, which has not been considered in this model. Instead we have to compute an "effective" yield limit to put into the equation instead of the full pressure-dependent yield curve. This is not trivial and will probably be different for various penetration processes.

However, if we for simplicity use the maximum yield limit, we should be able to get an idea on how the prediction of the modified Forrestal formula compares with the original one.

In Figure 4.2, we have compared the results from the Modified Forrestal approach with experimental data for penetration of the 75 mm and 152 mm projectiles against C30 targets. It is clear that the modified formula gives better agreement than the unmodified formula. There is, however, still some underprediction, although it is unclear whether the disagreement for the highest data point is just due to experimental scattering.

Comparing with Figure 4.1, we see that some boundary effects might be expected for the 152 mm projectile, as the experiments were carried out for $d_t/d = 160 \text{ cm}/7.5 \text{ cm} = 10.5$.

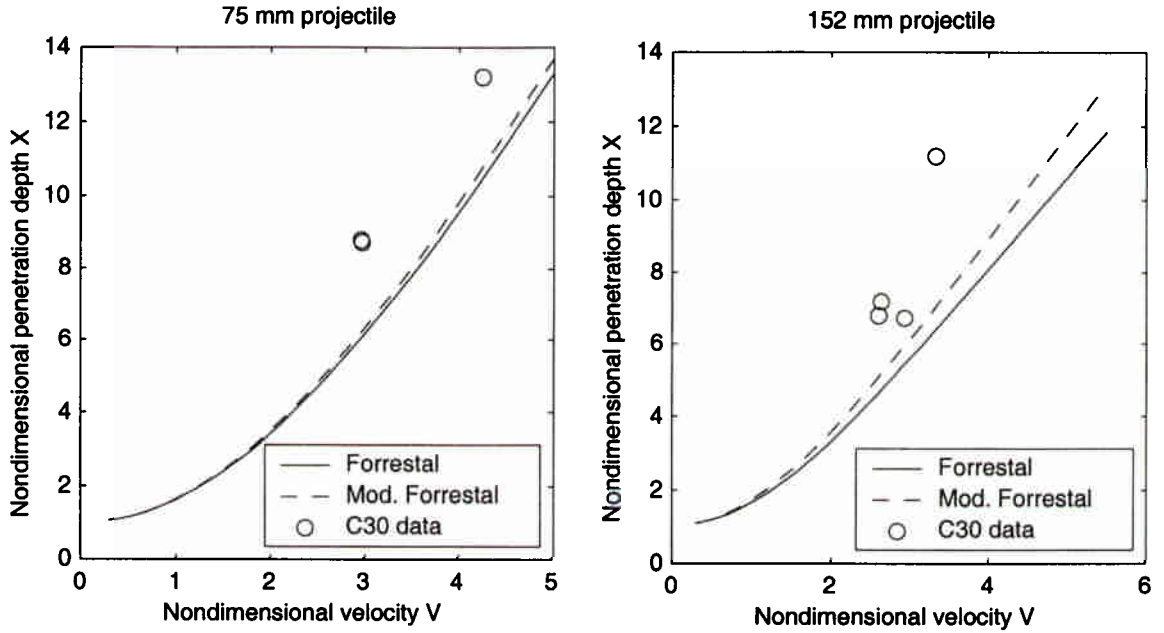


Figure 4.2: Experiments with 75 mm and 152 mm projectiles for C30 targets with $d_t/d = 21.3$ and $d_t/d = 10.5$ respectively. The data are compared with the modified Forrestal formula.

We also see that there is little difference between the modified and unmodified theory for the 75 mm projectile, which is not surprising considering that the experiments were carried out for $d_t/d = 160 \text{ cm}/7.5 \text{ cm} = 21.3$. However, there is still a potentially significant underprediction which might indicate boundary effects are present anyway. This could be due to other physical mechanisms not accounted for by this approach.

5 AUTODYN SIMULATIONS

Numerical simulations provide another method for checking whether boundary effects are present in an experiment, provided that the material models employed capture the relevant physical mechanisms. An advantage of simulations over the analytical methods presented in Chapter 4, is that we are able to use much more advanced material models in describing the concrete. However, this makes it necessary with more extensive material testing to obtain values for all the concrete parameters. Since such tests have mostly not been performed in the HPC experiments, we had to resort to using concrete models expected to have roughly similar properties.

Unless otherwise stated, all the simulations were performed using a Lagrange processor for the projectile and an Euler processor for the target. Concrete was modelled using a Porous Mohr–Coulomb model with a hydrodynamic tensile limit. The value of the tensile limit is difficult to measure experimentally. This is unfortunate, as it will be seen to be a very important parameter. As a first approximation, we have put this limit equal to the concrete tensile strength in our simulations. Details about the various concrete models are given in Appendix B.

To investigate boundary effects we have not only performed simulations of the actual experiments, but also varied the target diameter to see whether this influenced the results. Note that in the experiments the concrete targets were surrounded by a 3 mm steel jacket. This was not modelled in most of the simulations as we wanted to avoid including too many parameters at once when studying the physics of boundary effects. In experiments where boundary effects appeared to be present, we also performed additional simulations with the steel jacket included to see if this altered anything.

We will now describe the results of the various simulations and compare with experiments and analytical theory.

5.1 75 mm projectile against Densit

We will first look at experiments with the 75 mm projectile impacting C200 (Densit) targets. The triaxial concrete properties were measured with a GREAC cell at Imperial College and are given in Appendix A.

In the various experiments (97–5, 97–6, 97–7), the impact velocity was in the range 485–489 m/s. We have used a value of 485 m/s in our simulations.

In the three experiments, the target diameter was always 160 cm and the final penetration depth in the range 23.5 cm–25.0 cm. We ran simulations with a variety of target diameters. Since there was uncertainty in the input value for the hydrodynamic tensile limit, we also performed similar simulations with the same concrete without such a tensile limit to estimate the importance of this parameter. Results are given in Table 5.1.

Target diameter (cm)	Target/proj. diameter	Pen. depth (cm)	Pen. depth – no t.f.
36.0	4.8	38.8	28.5
40.0	5.3	36.5	27.3
56.4	7.5	26.9	24.3
71.4	9.5	24.2	23.6
103.0	13.7	23.1	23.1
130.4	20.5	23.0	23.0
180.0	24.0	23.0	23.0

Table 5.1: Results from simulations of penetration into Densit by a 75 mm projectile.

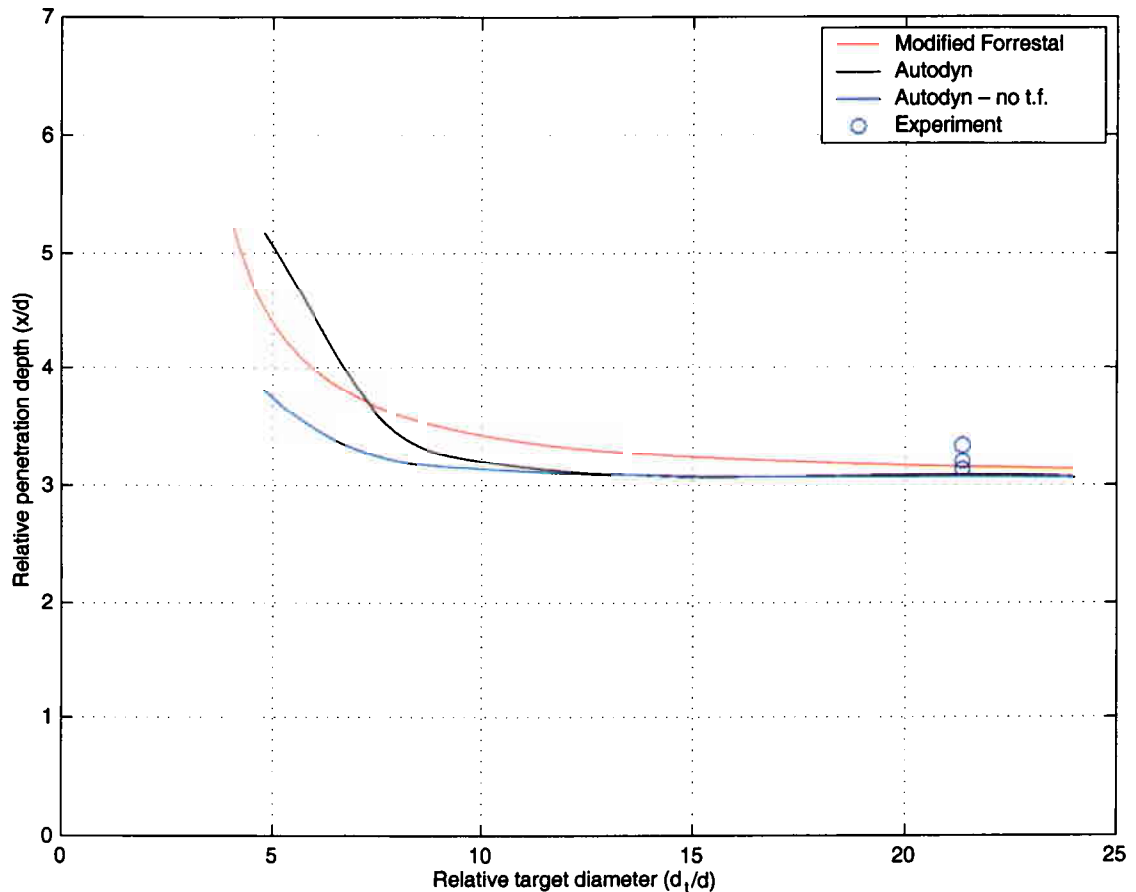


Figure 5.1: The relation between target diameter and penetration depth for a 75 mm projectile impacting Densit targets.

These results are also illustrated in Figure 5.1. Agreement between simulations, analytical theory and experiments is very good, which might be partly coincidental. However, in any case, it appears that in the HPC experiments for a target diameter of 160 cm, boundary effects had a negligible effect (if any) on the depth of penetration.

We also notice that the removal of the tensile failure limit has no influence on the penetration depth for the thick targets. However, as soon as the target diameter is small enough for boundary effects to come into play, the tensile limit becomes very important. For example, we see that there is a difference in penetration depth of more than 35% for a target of diameter 36 cm.

Thus, we have identified the tensile limit as a very important parameter in the determination of boundary effects. As we have seen, this parameter is not included in any of the analytical approaches.

5.2 75 mm projectile against C150

Several experiments were also performed with firing the 75 mm projectile against C150 targets. In most of the experiments perforation was achieved, which is beyond the scope of this report. However, in 99-4, 99-5 and 99-6 the target had a length of 80 cm, which was

enough for the projectile to stop inside the target. The impact velocities were 612 m/s, 619 m/s and 620 m/s and the target diameter was 140 cm.

The experiments revealed a relatively large scattering of the final penetration depth of $\pm 10\%$. The results were 45 cm, 51 cm and 54 cm, even though experimental parameters were identical (except for minor changes in the impact velocity, which clearly is not the reason for the different results).

Target Diameter (cm)	Target/Projectile diameter	Penetration Depth (cm)
70	9.3	64.3
101	13.5	51.2
140	18.7	39.5
202	26.9	34.7
252	33.6	33.5

Table 5.2: Results from simulations of penetration into C150 by a 75 mm projectile.

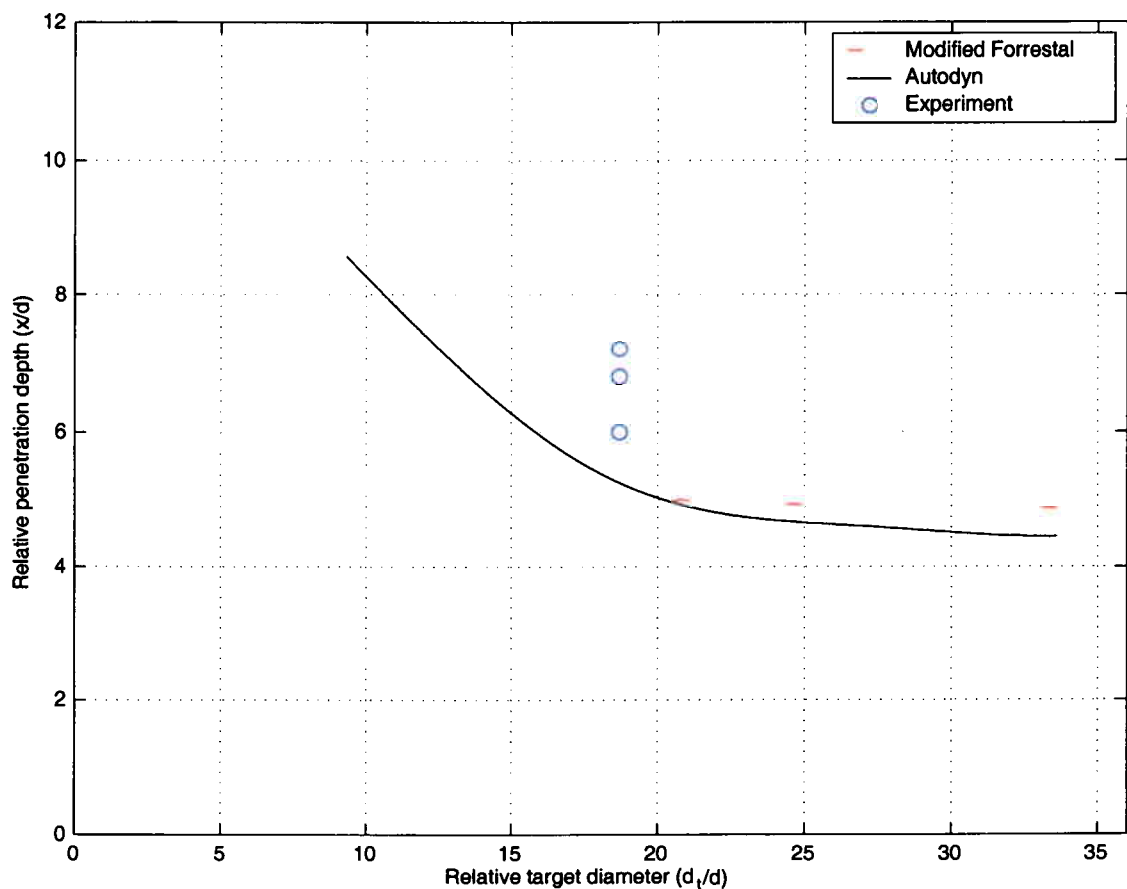


Figure 5.2: The relation between target diameter and penetration depth for a 75 mm projectile impacting C150 targets.

Unfortunately, no triaxial testing was performed of the particular C150 concrete used in the experiments, so in our simulations we have used a modified version of a C140 concrete

model by Hanchak (3). Our results for different target diameters and an impact velocity of 615 m/s are given in Table 5.2, and shown graphically in Figure 5.2.

We see that the simulations seem to underpredict the penetration depth. However, from the simulations there appears to be some indications that boundary effects might have been present in the experiments. The modified Forrestal approach does not seem to indicate significant boundary effects, though.

5.3 75 mm projectile against standard concrete

The 75 mm projectile was also fired against standard concrete with impact velocities of 482 m/s and 483 m/s (97-3,97-4). The concrete compressive strength was measured to be 38 MPa. Since no triaxial material tests were performed for that particular concrete, we use triaxial data for another concrete (DRA-9276) that should have roughly the same properties.

In the simulations we used an impact velocity of 483 m/s. Results for different target diameters are given in Table 5.3 and are shown graphically in Figure 5.3.

Target Diameter (cm)	Target/Projectile diameter	Penetration Depth (cm)
61	8.1	118.4
100	13.3	91.0
160	21.3	79.7
200	26.7	78.7
280	37.3	78.3

Table 5.3: Results from simulations of penetration into standard concrete by a 75 mm projectile.

The experimental results were 65.5 cm and 66.0 cm, so our simulation result of 79.7 cm is about 20% too high. Forrestal's formula predicts a penetration depth of 51 cm, which is too small. This could be an indication of boundary effects, but from the simulations these appear to be very small and probably not measurable in an experimental situation.

5.4 152 mm projectile against Densit

Next we examine penetration of the 152 mm projectile into Densit targets. Two such experiments (98A-5, 98A-6) have been performed at impact velocities of 480.0 m/s, both giving consistent penetration depths of 45.0 cm for a target of diameter 160 cm.

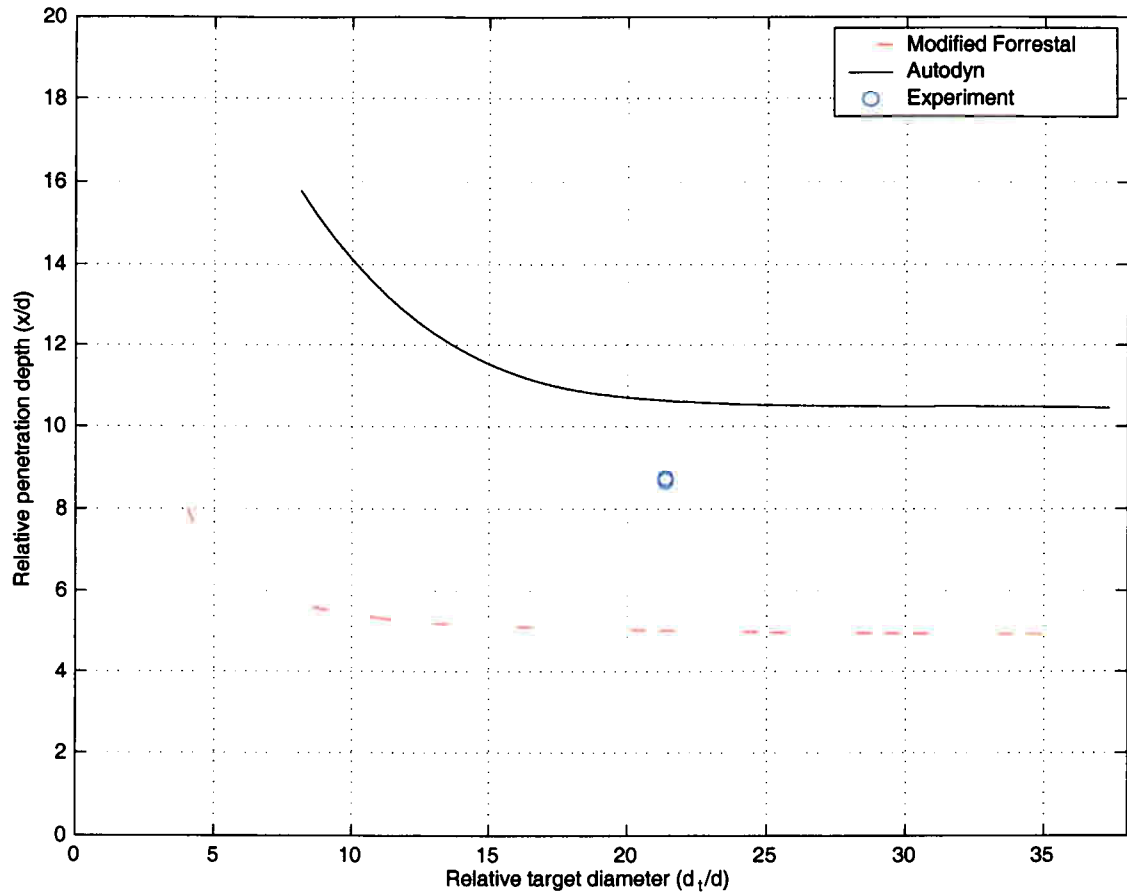


Figure 5.3: The relation between target diameter and penetration depth for a 75 mm projectile impacting C30 targets.

The simulation results are shown in Table 5.4 and Figure 5.4, and are seen to predict smaller penetration depths than were experimentally measured. The agreement between theory and experiment therefore does not seem to be very good. However, in any case, there is nothing to indicate that significant boundary effects were present in the experiments.

Target Diameter (cm)	Target/Projectile diameter	Penetration Depth (cm)
58	3.8	41.0
100	6.6	33.0
160	10.5	29.8
250	16.4	29.1

Table 5.4: Results from simulations of penetration into Densit by a 152 mm projectile.

Finally, we also simulated experiment 98B-7 where the same projectile was fired at an impact velocity of 579.8 m/s. The experimental result for the penetration depth was 53.0 cm while our simulation gave only 39.7 cm.

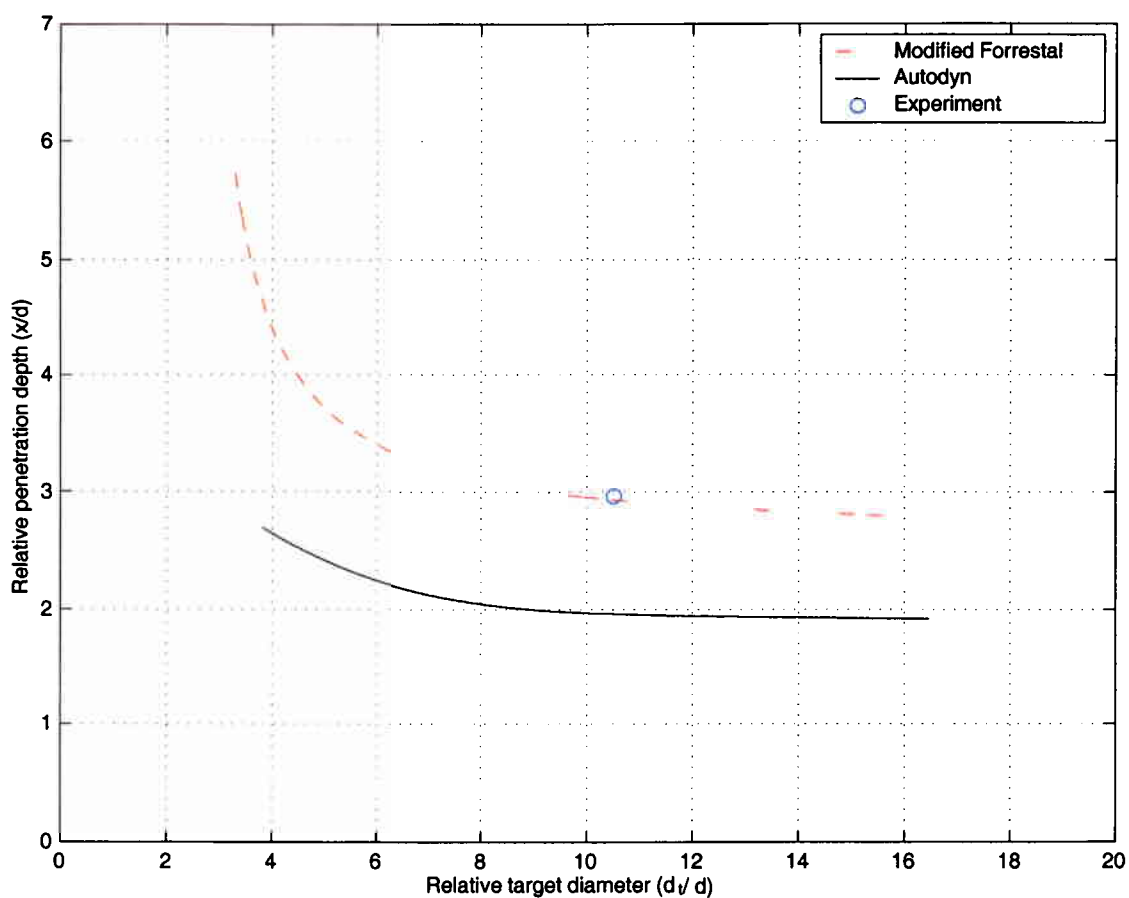


Figure 5.4: The relation between target diameter and penetration depth for a 152 mm projectile impacting a Densit target at 480 m/s.

5.5 152 mm projectile against C150

Finally we examine penetration into C150 concrete targets by the 152 mm projectile. Several experiments (99–13, 99–15, 99–16, 99–17) have been performed on this concrete for the same experimental conditions except for a varying target diameter. These tests are therefore very useful in the investigation of boundary effects.

The impact velocity was in the range 465–468 m/s, and in the numerical simulations we have used 465 m/s. The experimental and numerical results are given in Table 5.5 and plotted in Figure 5.5.

Target diameter (cm)	Target/projectile diameter	Pen. depth (cm) (Numerical)	Pen. depth (cm) (Experimental)
100	6.6	52.5	75
160	10.5	41.3	66
240	15.8	35.6	38
300	19.7	33.1	44

Table 5.5: Experimental results for penetration of 152 mm projectile into C150 concrete targets of various diameters at 465–468 m/s.

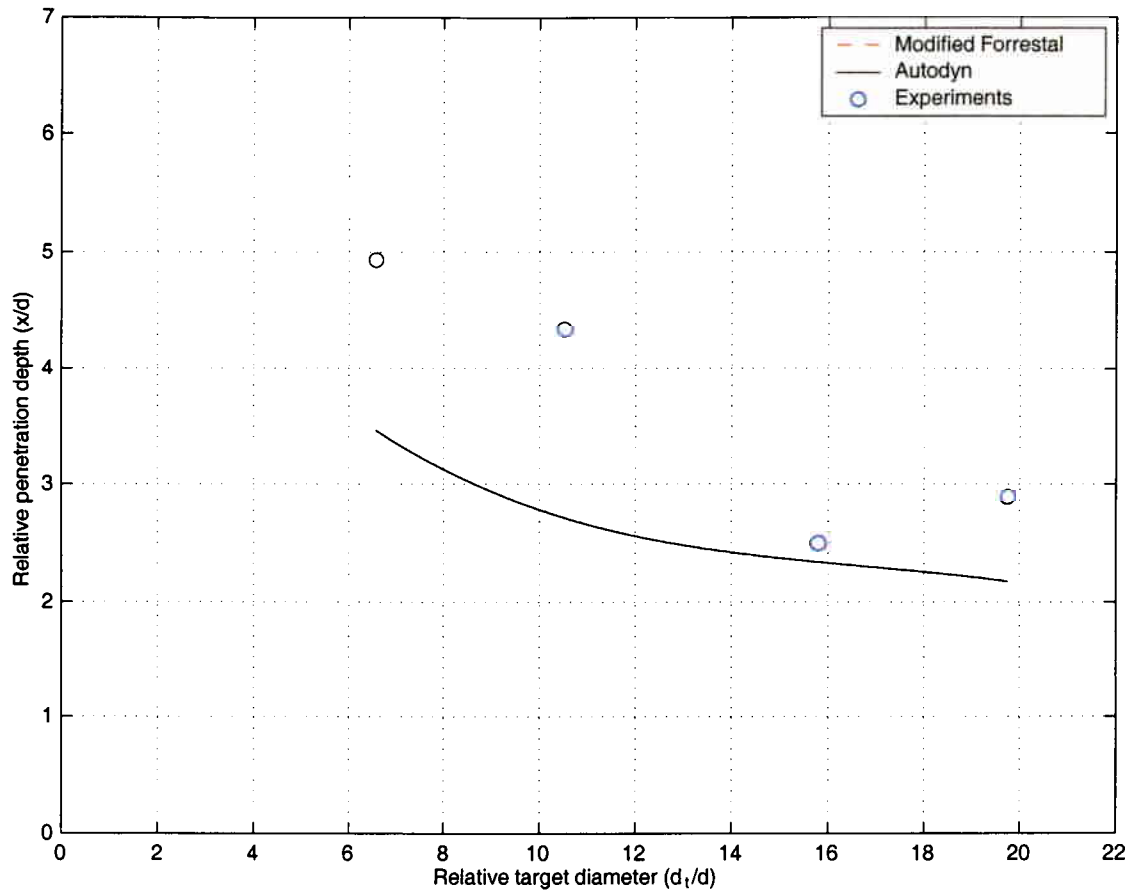


Figure 5.5: The relation between target diameter and penetration depth for a 152 mm projectile impacting C150 targets at 465 m/s.

We clearly see both from the experiments and simulations that there are boundary effects for the two smallest targets. This is also obvious from Figure 5.6, which shows the 100 cm and 240 cm targets after impact of the projectile. The small target is almost completely destroyed, while the large target only has a few radial cracks going out to the boundary. Experimental uncertainties are probably the reason that we achieve a larger penetration depth for the 240 cm target than for the 300 cm target.

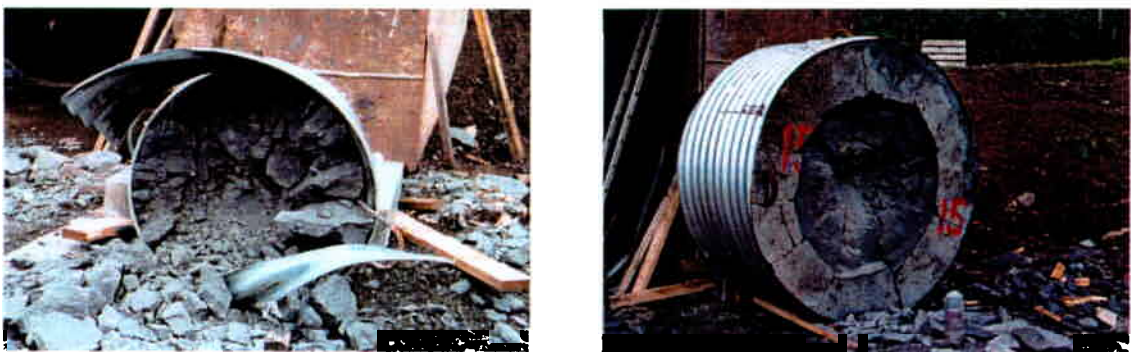


Figure 5.6: The 100 cm and 240 cm C150 targets after impact of the 152 mm projectile.

To see how important the value of the hydrodynamic tensile limit was, we ran some simulations where it was set to -8.0 MPa, which meant tensile failure was less likely to occur.

We also tried using a crack softening of 162 J/m^2 to see if this had any effect. Results are given in Table 5.6:

Target diameter (cm)	Pen. depth (cm) (crack soft.)	Pen. depth (cm) (no c.s.)
100	49.0	49.0
300	33.5	33.3

Table 5.6: Penetration depth for two different target diameters for an increased tensile failure limit, both with and without crack softening.

We see that introducing crack softening did not influence the results significantly, but again the value of the hydrodynamic tensile limit changed the results for the small target diameter when boundary effects were present. However, the simulations clearly still predict less boundary effects than the experiments.

5.5.1 Results for a different C150 material model

As mentioned, we had no exact material data for the C150 concrete, so our numerical input data was obtained by modifying a concrete model by Hanchak. To see if similar numerical results would be obtained for a different concrete model, we tried a different approach at finding a C150 model.

We started with the Densit material model and made it weaker by calibrating the Mohr–Coulomb yield curve with the C150 penetration experiments. For a target of diameter 250 cm, we found that a decrease of the Densit yield curve by 40% gave a penetration depth of 41.8 cm, which was in reasonable agreement with the experiments. The new C150 Mohr–Coulomb yield curve is given in the Appendix B.

It was now examined whether there would be boundary effects with the new model, so the Autodyn simulations shown in Table 5.7 were performed.

Target diameter (cm)	Penetration depth (cm)
100	48.6
160	43.7
250	41.8

Table 5.7: Results of Autodyn simulations against C150 targets of various diameters.

It is immediately clear that, even after accounting for the experimental uncertainties, the Autodyn simulations here predict significantly less influence from boundary effects than what was seen in the experiments.

Also the new C150 material model is even less sensitive to the target diameter than the original concrete model.

This could be due to a too high value for the hydrodynamic tensile limit being used. As we have seen earlier, the value of this parameter can be very important if there are boundary effects. To investigate this further, we performed a sensitivity analysis of the importance of the hydrodynamic tensile limit for a target with 100 cm diameter. Results are given in Table 5.8.

Tensile limit (MPa)	Penetration depth (cm)
1.0	69.0
2.6	68.0
5.0	67.9
10.0	63.9
18.0	51.5
26.0	48.6

Table 5.8: Sensitivity analysis of boundary effects to the hydrodynamic tensile limit.

As expected, the results are quite sensitive to the value of the hydrodynamic tensile limit. Therefore, it is possible that good agreement would have been found between Autodyn and experiment, if the correct value of this limit had been known. However, without having the material data for this specific C150 concrete, this is impossible to tell for sure.

5.6 152 mm projectile against standard concrete

The 152 mm projectile was also fired at standard concrete with a compressive strength in the range 30–41 MPa (98A–1, 98B–2, 99–14, 99–18). The impact velocities were in the range 466–481 m/s, and target diameter was 160 cm, except in 99–14 where it was 240 cm.

Experimental penetration depths were 102 cm, 103 cm and 109 cm for the 160 cm diameter targets and 101 cm for the 240 cm target. Simulations were performed at an impact velocity of 480 m/s and results are presented in Table 5.9 and Figure 5.7.

Target diameter (cm)	Target/ proj. diameter	Pen. depth (cm) with steel	Pen. depth (cm) with steel, no t.f.	Pen. depth (cm) without steel	Pen. depth (cm) without steel, no t.f.
75.0	4.9	136.5	149.2	196.7	185.5
120.0	7.9	119.7	124.6	139.9	137.2
160.0	10.5	106.8	110.8	118.3	119.1
194.0	12.8	101.8	102.0	109.4	109.3
250.0	16.4	99.0	99.1	103.8	103.7
310.0	20.4	98.8	98.8	101.6	101.6

Table 5.9: Results from simulations of penetration into standard concrete by a 152 mm projectile.

The numerical results seem to indicate that boundary effects might actually have been present in these experiments. The simulations show a difference in penetration depths of roughly 17% for target diameters of 160 cm and 310 cm. This view is slightly strengthened by the experimental results where the smallest penetration depth was obtained for the largest target, although this difference is very small and could be due to experimental uncertainties. Agreement between simulations and experiment is seen to be quite good, though.

The concrete target was surrounded by a 3 mm thick steel jacket which was not modelled in the first simulations. Since boundary effects looked to be present, we ran the simulations also with the steel jacket included to see if this had any effect. These results are also given in Table 5.8 and Figure 5.7. We notice that the steel confinement is seen to be quite important, especially when the target diameter is small, which is when boundary effects are present.

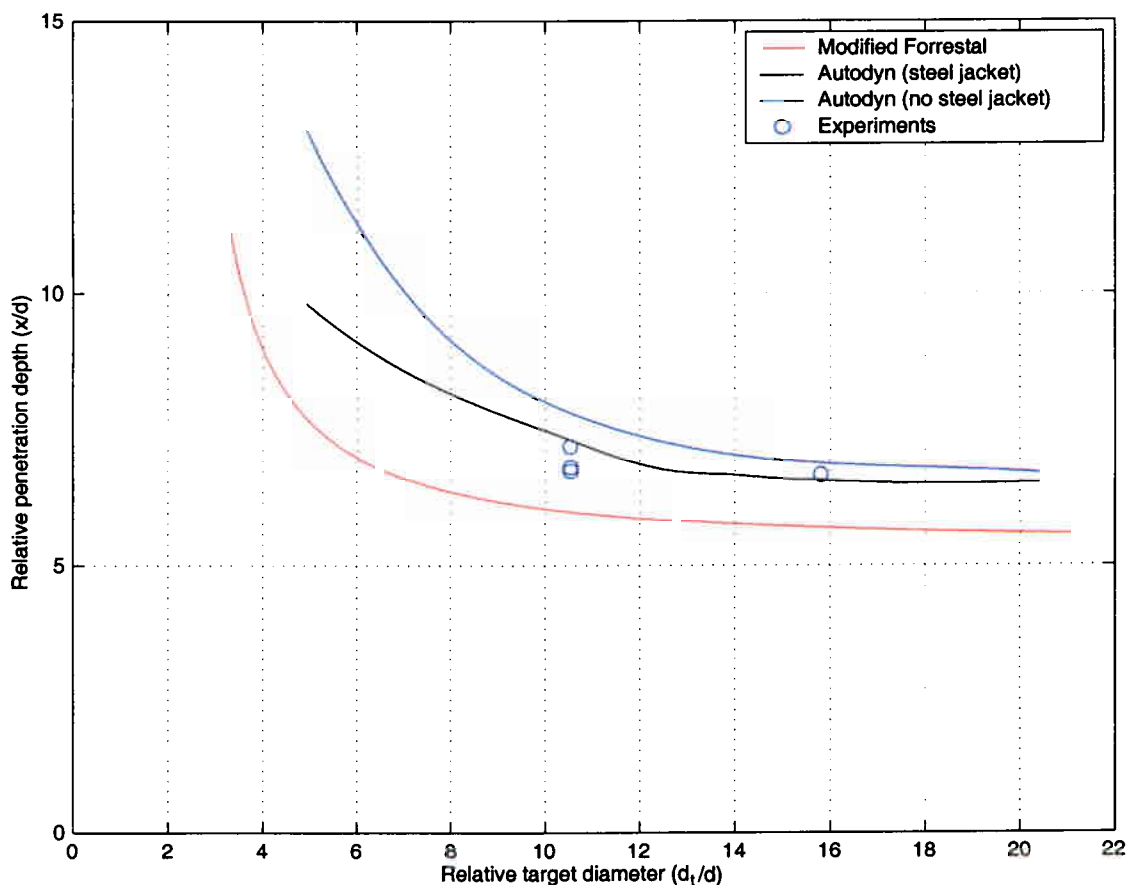


Figure 5.7: The relation between target diameter and penetration depth for a 152 mm projectile impacting C30 targets at 480 m/s.

However, there are some surprising results. In particular that for certain target diameters the removal of the tensile failure limit resulted in increased penetration depths when steel confinement was present. At the moment we have no physical explanation for this, but we can not rule out that it is due to a numerical effect. This will be further investigated.

5.7 Comparison of numerical and experimental results

In Table 5.10 we present a comparison between the simulation results and the experimental results.

	75 mm	152 mm
C30	+21%	+2%
C150	-21%	-37%
Densit	-5%	-34%

Table 5.10: Comparison of numerical and experimental results.

It is clear that the numerical results are not quite as good as hoped. This could be due to inadequate concrete material models being used, as for C30 and C150 we have only made an educated guess at the concrete model. However, even for Densit where data is available, the numerical predictions are much too low for the 152 mm projectile, although pretty accurate for the 75 mm projectile. In fact, on comparing the results for both projectiles, it is seen that the 152 mm projectile simulations always underpredicts more or overpredicts less than the 75 mm projectile simulations. However, preliminary simulations with the more advanced RHT material model indicate that better agreement with experiment can be obtained. This will be further investigated.

6 FURTHER NUMERICAL ANALYSIS OF BOUNDARY EFFECTS

In this chapter we examine the penetration process more closely to see whether this will give us any further clues to the physics behind boundary effects.

6.1 75 mm projectile against Densit

We first look at the time–history of the 75 mm projectile against Densit to see when boundary effects first appear. The velocity and acceleration plot for the projectile are illustrated in Figure 6.1.

It is seen that the velocities are equal in the beginning, but then they diverge after a while. How early they diverge depends on the target diameter. The acceleration plot shows the same thing as the velocity plot, but the trend is even more obvious. The force/acceleration is the same at first, but then something happens and the force is reduced by an amount depending on the degree of confinement of the target.

Let us examine this observation a little further. We denote the acceleration of the projectile penetrating the 153.6 cm diameter target by a_0 , and the acceleration of a similar projectile penetrating a target of different diameter by a_d . The relative acceleration of the two projectiles is then defined by $\Delta a_d = a_d - a_0$. In Figure 6.2, we have plotted the relative accelerations for the various projectiles. The information content is the same as in the pre-

vious plot, but the points where the curves start to diverge are maybe seen even more explicitly here.

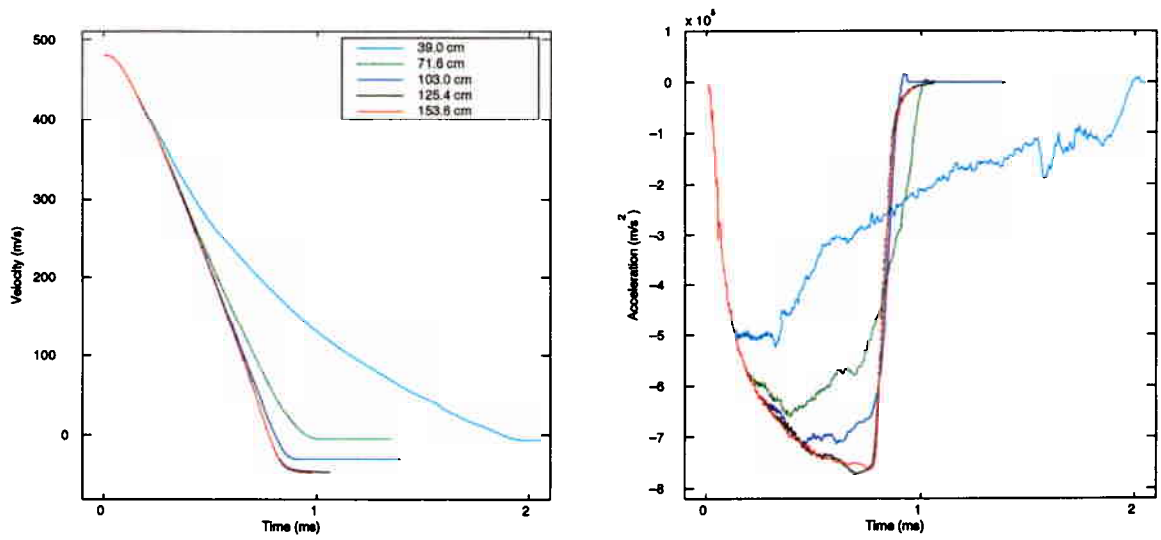


Figure 6.1: Velocity and acceleration plots for penetration of 75 mm projectile into Densit.

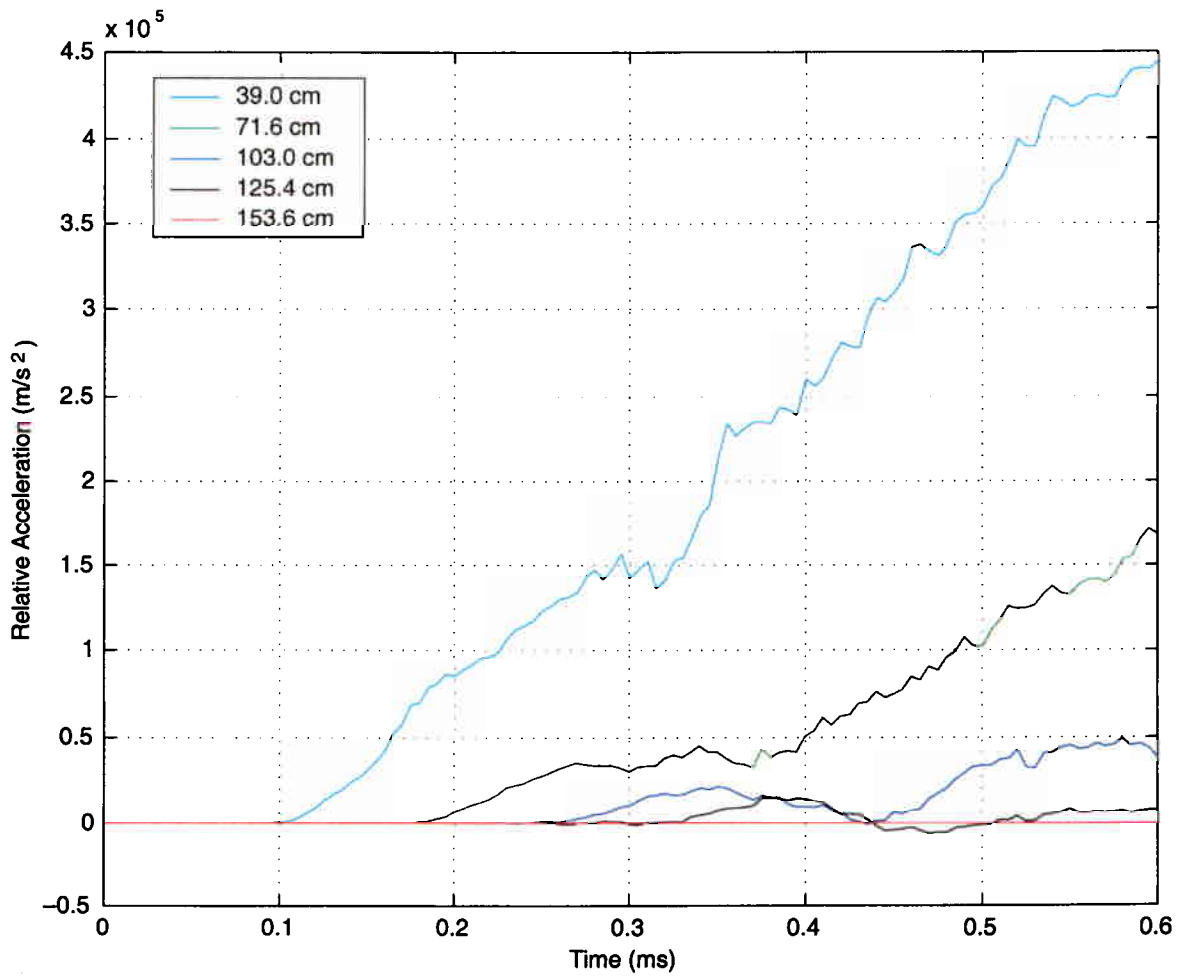


Figure 6.2: Relative acceleration as a function of time for various target diameters for penetration of 75 mm projectile into Densit.

If we focus on the graph for $d_t = 39.0\text{cm}$, we see that the acceleration starts to increase after about 0.11 ms. The velocity of an elastic wave in Densit is around 3800 m/s. This means that the time for a wave to make the roundtrip from the projectile to the target boundary and back again, would be roughly $T = \frac{0.39}{3800} \text{ s} = 0.103 \text{ s}$, which corresponds almost exactly to when the reflected waves reach the projectile. The same can easily be shown for the other target diameters. This strengthens the view that boundary effects are due to reflected waves from the target boundary.

6.2 75 mm projectile against C30

To see if this holds true also in other cases, we also examined the penetration process for the 75 mm projectile against C30 concrete more closely.

In Figure 6.3 we have again plotted velocity and acceleration as a function of time for the various target diameters, and again we see that the penetration processes are identical in the beginning until boundary effects set in. This is even more evident in Figure 6.4. which shows the relative acceleration.

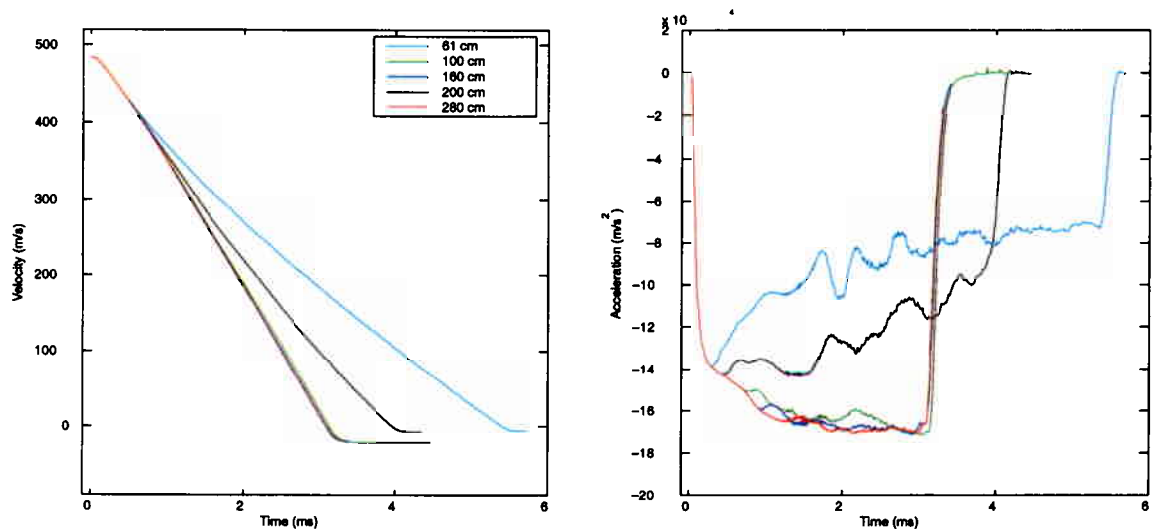


Figure 6.3: Velocity and acceleration plots for penetration of 75 mm projectile into C30.

Again we can identify the point when the curves start to diverge with the return of reflected waves from the boundary. The velocity of an elastic wave in our C30 model is about 2370 m/s, which means it should take $0.61/2370 \text{ s} = 0.257 \text{ ms}$ to travel from the center of the target out to the boundary and back again. Close inspection of Figure 6.4 reveals that the curve diverges almost exactly at this time, and the same is seen to be true for the other curves.

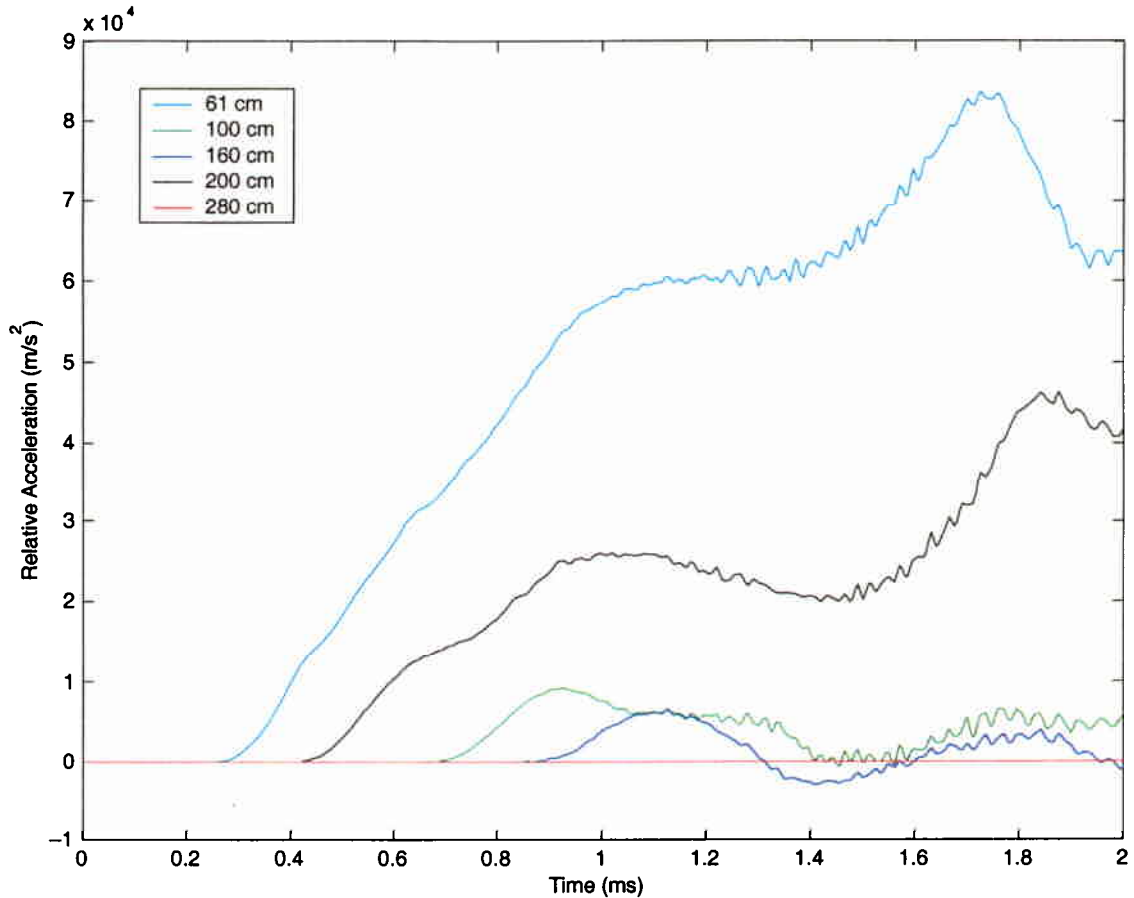


Figure 6.4: Relative acceleration as a function of time for various target diameters for penetration of 75 mm projectile into Densit.

The general trend is clear. If the target has a sufficiently large diameter, the force (acceleration) rises to its peak and stays approximately constant during the whole process. This is best seen in simulations that last for a sufficiently long period, like penetration into the weak C30 concrete. However, if the target is not large enough, the force might never reach the peak level, and further it starts decreasing during the penetration process instead of remaining constant.

7 RESULTS, RECOMMENDATIONS AND FURTHER WORK

It is difficult to describe the influence of boundaries in a precise manner, since several complex mechanisms may contribute to the total effect. So far, no completely satisfactory analytical condition has been found. The modified Forrestal approach looks promising, but unfortunately it is at the moment based on a Mises material model. This approach also ignores the effects due to tensile failure, which is believed to be important. Possible extensions of this model should involve using a Mohr–Coulomb material model for the concrete and accounting for the effects of scabbing and spalling due to material failure. This is an ongoing work at FFI.

On the numerical side, we have seen that it is possible to predict boundary effects qualitatively using Autodyn. However, it is uncertain how good these predictions are quantita-

tively, as they have been performed using a rather basic material model with a simple hydrodynamic tensile limit. It is very important, but not trivial, to select a representative value of this parameter. Probably a more advanced tensile failure criterion, including strain softening and fracture energy in some way, should be employed. There should also be a coupling between the tensile failure and some sort of damage variable in the model to account for the modified material behaviour in compression and shear. Such features are e.g. found in the RHT-model for AUTODYN and model #72 in LS-DYNA, as well as others. These issues will be studied more closely in the future.

In the end, the problem of boundary effects comes down to the problem of modeling concrete adequately. At the time of writing, high quality numerical simulations seem to be necessary in order to give reliable quantitative answers. It will be difficult to capture the physics only by using analytical models. However, it is possible that analytical models, such as a modified Forrestal formula with an improved material model, in the future could be used to estimate the necessary target diameter.

At the moment, though, only very rough guidelines for determining a sufficiently large target size in a penetration experiment can be given. Drawing on our experience with the analytical and numerical tools and the experimental data, it appears that with a target size satisfying $d_t/d = 15$, one should be reasonably safe of avoiding boundary effects in most cases.

References

- (1) Pullen A D, Testing of Fibre-Reinforced Concrete Materials Using the GREAC-cell, CRIC Client Report CRIC/98/FFI/1, September 1998
- (2) Forrestal M J, Altman B S, Cargile J D, Hanchak S J, An Empirical Equation for Penetration depth of Ogive Nose Projectiles into Concrete Targets, Int. J. Impact Engng Vol 15, No.4, pp. 395-405, 1994
- (3) Hanchak S J, Forrestal M J, Young E R, Ehrgott J Q, Perforation of Concrete Slabs with 48 MPa and 140 MPa Unconfined Compressive Strengths, Int J Impact Engng, Vol 12, No 1, 1992
- (4) Sjøel H, Teland J A, Prediction of Concrete Penetration using Forrestal's Formula, FFI/RAPPORT-99/04415
- (5) Littlefield D L, Anderson C E, Partom Y, Bless S J, The Penetration of Steel Targets Finite in Radial Extent, Int. J. Impact Engng Vol 19, No. 1, pp. 49-62, 1997
- (6) Teland J A, A Review of Analytical Penetration Mechanics, FFI/RAPPORT-99/01264
- (7) Pullen A D, Newman J B, Dynamic Properties of Shocked Geological Materials, Final Technical Report, Imperial College

APPENDIX

A CONCRETE DATA

The concrete material models used in the various Autodyn simulations are described in this chapter. All of the concretes were modelled using a Porous Equation of state and a Mohr–Coulomb yield condition.

A.1 C30 model

No triaxial tests were performed to provide data for the C30 concrete used in the experiments. Therefore, we used the model DRA–9276 in (7), which had roughly the same compressive strength and was expected to have similar properties. Data for the EOS and yield curve are given in Tables A.1 and A.2.

Density (kg/m ³)	Pressure (MPa)
1957	0
1974	18.5
2098	81.3
2257	183.7
2313	262.9

Table A.1: EOS data for the C30 concrete model.

Pressure (MPa)	Yield Stress (MPa)
0	6.7
33	50
120	110
250	165

Table A.2: Yield curve data for the C30 concrete model.

The other material parameters were set as follows:

Shear modulus	4.0 GPa
Hydrodynamic tensile limit:	–3.47 MPa
Reference density:	2221.6 kg/m ³
Solid sound speed:	1729 m/s
Porous sound speed:	1729 m/s

A.2 C150 model

No triaxial material tests were performed for the C150 concrete either, so we had to use a slightly modified version of a C140 concrete model in (3). EOS and yield curve data are given in Tables A.3 and A.4.

Density (kg/m ³)	Pressure (MPa)
2700	150
2800	250
2900	500
3000	800
3100	1100
3200	1500
3300	2000

Table A.3: EOS data for the main C150 concrete model.

Pressure (MPa)	Yield Stress (MPa)
0	20
25	113.1
50	150.9
100	202.5
200	273.0
300	325.6
400	369.3
600	441.2
800	500.8
1000	552.6

Table A.4: Yield curve data for the main C150 concrete model.

The other material parameters were set as follows:

Shear modulus	25.0 GPa
Hydrodynamic tensile limit:	-8.0 MPa
Reference density:	3050 kg/m ³
Solid sound speed:	3000 m/s
Porous sound speed:	2720 m/s

We also created another C150 model by calibrating the Densit model to the penetration experiments. The yield curve of the new “artificial” C150 model is given in Table A.5, while all other parameters were left unchanged from the Densit model.

Pressure (MPa)	Yield Stress (MPa)
0	60
50	96
200	180
350	240

Table A.5: Yield curve data for the “artificial” C150 concrete model.

A.3 Densit model

To determine the properties of the Densit concrete, samples were tested at Imperial College, London using a GREAC–cell. The complete results of this test are described in Pullen (1). The data was also given in a form suited to implementation in the hydrocode Autodyn.

However, from inspection of the report it was concluded that the given value of the shear modulus $G = 5.28$ GPa was incorrect. Instead a value of $G = 15.0$ GPa was extracted from the curves in (1) and used in the numerical simulations. The velocity of sound was also corrected for, and the value of 2720 m/s was used.

Unfortunately, the GREAC–cell test could only provide material data for pressures up to 347.6 MPa. Based on our experience and some educated guessing, the EOS was there extrapolated to higher pressures. The EOS and the yield curve are given in Tables A.6 and A.7.

Pressure (MPa)	Density (kg/m ³)
0	2884.0
65.3	2893.9
89.0	2907.1
248.0	2955.2
1148.9	3200.0

Table A.6: EOS data for the Densit model.

Pressure (MPa)	Yield Stress (MPa)
0	100
50	160
200	300
350	400

Table A.7: Yield curve data for the Densit model.

The other material parameters were set as follows:

Shear modulus	15.0 GPa
Hydrodynamic tensile limit:	–25.6 MPa
Reference density:	2992 kg/m ³
Solid sound speed:	2720 m/s
Porous sound speed:	2720 m/s

B EXPERIMENTAL PENETRATION DATA

Shot number	v [m/s]	x [mm]	σ_c [MPa]	Target diameter [cm]	Target thickness [cm]	Residual velocity [m/s]	d _f /d	Remarks
97-1	484	680	38	160	10 x 20	0	21,3	
97-2	480	200	200	150	5 x 20	0	20,0	2,0F S
97-3	483	655	38	160	200	0	21,3	
97-4	482	660	38	160	200	0	21,3	
97-5	485	250	180	160	100	0	21,3	2,0F
97-6	489	235	180	160	100	0	21,3	2,0F
97-7	485	240	180	160	50	0	21,3	2,0F
98B-10	571,1	410	90	160	?	0	21,3	F
98B-11	652,9	560	90	160	150	0	21,3	1,0F
98B-12	647,1	440	140	160	120	0	21,3	1,0F
98B-13	649,8	440	200	150	4 x 20	0	20,0	2,0F S
98B-9	646,8	990	30	160	200	0	21,3	
99-1	617		153	140	40	276	18,7	
99-2	618		153	140	40	303	18,7	
99-3	618		153	140	40	293	18,7	
99-4	620	450	153	140	80	0	18,7	
99-5	612	540	153	140	80	0	18,7	
99-6	619	510	153	140	80	0	18,7	
99-7	617		153	140	40	Not measured	18,7	R
99-8	616		153	140	40	Not measured	18,7	R
99-9	619		153	140	40	260	18,7	R



Table B.1: Penetration experiments with 75 mm projectiles. F=Fiber (number indicates percentage of fiber), S=Square target cross section, R = Reinforcement.

Shot number	v [m/s]	x [mm]	σ_c [MPa]	Target diameter [cm]	Target thickness [cm]	Residual velocity [m/s]	d _f /d	Remarks
96B-1	476		250	150	4 x 20	approx. 0	9,9	F
96B-2	478		36	150	5 x 20	160	9,9	
96B-3	478	350	220	150	5 x 20	0	9,9	4,0F R
96B-4	473	600	180	150	5 x 20	0	9,9	F R
98A-1	467,6	1030	41	160	300	0	10,5	
98A-2	480,8	460	250	220	5 x 20	0	14,5	F
98A-3	479,7	300	200	150	100	0	9,9	1,5F R S
98A-4	481,4	670	34	150	2 x 100	0	9,9	R
98A-5	480	450	203	160	120	0	10,5	
98A-6	480,3	450	200	160	100	0	10,5	F
98A-7	479,2	630	90	160	150	0	10,5	
98A-8	486,2	590	108	160	150	0	10,5	1,0F
98A-9	488,2	560	83	160	150	0	10,5	1,5F
98B-1	575,5	1700	36	160	300	0	10,5	
98B-2	480,7	1020	30	160	300	0	10,5	
98B-3	480,3	595	140	160	120	0	10,5	1,0F
98B-4	480,3	420	140	150	120	0	9,9	1,0F R S
98B-5	584	810	140	160	150	0	10,5	1,0F
98B-6	582,9	980	90	160	150	0	10,5	
98B-7	579,8	530	200	160	150	0	10,5	2,0F
98B-8	580,8	830	132	160	150	0	10,5	
99-13	465	440	149	300	120	0	19,7	
99-14	468	1010	39	240	200	0	15,8	
99-15	468	380	149	240	120	0	15,8	
99-16	467	660	153	160	120	0	10,5	
99-17	466	750	153	100	120	0	6,6	
99-18	466	1090	39	160	200	0	10,5	
99-19	464	570	120,5	160	120	0	10,5	1,0F
99-20	467	500	120,5	160	120	0	10,5	1,0F R
99-21	576	790	158	160	150	0	10,5	G
99-22	573	440	158	160	150	0	10,5	Fail

Table B.2: Penetration experiments with 152 mm projectiles. G=Granite.

DISTRIBUTION LIST

FFIBM Dato: 9 November 2000

RAPPORT TYPE (KRYSS AV)			RAPPORT NR	REFERANSE	RAPPORTENS DATO			
<input checked="" type="checkbox"/>	RAPP	<input type="checkbox"/>	NOTAT	<input type="checkbox"/>	RR	2000/05414	FFIBM/766/130	9 November 2000
RAPPORTENS BESKYTTELSESGRAD				ANTALL EKS UTSTEDT	ANTALL SIDER			
UNCLASSIFIED				54	34			
RAPPORTENS TITTEL				FORFATTER(E)				
BOUNDARY EFFECTS IN PENETRATION INTO CONCRETE				TELAND Jan Arild, SJØL Henrik				
FORDELING GODKJENT AV FORSKNINGSSJEF:				FORDELING GODKJENT AV AVDELINGSSJEF:				
								

EKSTERN FORDELING

INTERN FORDELING

ANTALL	EKS NR	TIL	ANTALL	EKS NR	
1		FBT/S	14		FFIBIBL
1		v/ Helge Langberg	1		Adm direktør/stabssjef
1		v/ Gro Markeset	1		FFIE
1		v/ Leif Riis	1		FFISYS
			5		FFIBM
1		FOI	1		Bjarne Haugstad FFIBM
		S-14725 TUMBA	1		Svein Rollvik FFIS
		Sverige	1		Eirik Svinsås FFIBM
1		v/ Anders Carlberg	1		Haakon Fykse FFIBM
1		v/ Lennart Ågårdh	1		Åge Andreas Falnes Olsen FFIBM
1		v/ Håkan Hansson	1		John F Moxnes FFIBM
1		v/ Mattias Unosson	1		Knut B Holm FFIBM
1		v/ Johan Magnusson	2		Henrik Sjøel FFIBM
			2		Jan Arild Teland FFIBM
1		HKV/KRI Plan/Anläggning			
		SE-10785 STOCKHOLM			
		Sverige			FFI-veven
1		v/ Ingvar Anglevik			
1		Forv-M			
		S-63189 ESKILSTUNA			
		Sverige			
1		v/ Bjørn Lindberg			
1		v/ Leif Ekblom			
1		TNO			
		Lange Kleiweg 137			
		P. O. Box 45			
		2280 AA RIJSWIJK			
		Nederland			
1		v/ Jaap Weerheijm			
1		v/ Cyril Wentzel			

EKSTERN FORDELING**INTERN FORDELING**

ANTALL	EKS NR	TIL	ANTALL	EKS NR
1		DERA X107, Barnes Wallis Building Farnborough		
1		v/ Cathy O'Carroll		
1		v/ Jim Sheridan		
		 www.ffi.no		